

Vector Transport Free Riemannian LBFGS for Optimization on Symmetric Positive Definite Matrix Manifolds

Reza Godaz^{1,*}, Benyamin Ghogh^{2,*}, Reshad Hosseini³, Reza Monsefi¹, Fakhri Karray², Mark Crowley²

¹Department of Computer Engineering, Ferdowsi University of Mashhad, Mashhad, Iran

²Department of Electrical and Computer Engineering, University of Waterloo, Waterloo, ON, Canada

³Department of Electrical and Computer Engineering, University of Tehran, Tehran, Iran

Emails: reza.godaz@mail.um.ac.ir, bghogh@uwaterloo.ca, reshad.hosseini@ut.ac.ir, monsefi@um.ac.ir, karray@uwaterloo.ca, mcrowley@uwaterloo.ca

Abstract—This work concentrates on optimization on Riemannian manifolds. The Limited-memory Broyden–Fletcher–Goldfarb–Shanno (LBFGS) algorithm is a commonly used quasi-Newton method for numerical optimization in Euclidean spaces. Riemannian LBFGS (RLBFGS) is an extension of this method to Riemannian manifolds. RLBFGS involves computationally expensive vector transports as well as unfolding recursions using adjoint vector transports. In this article, we propose two mappings in the tangent space using the inverse second root and Cholesky decomposition. These mappings make both vector transport and adjoint vector transport identity and therefore isometric. Identity vector transport makes RLBFGS less computationally expensive and its isometry is also very useful in convergence analysis of RLBFGS. Moreover, under the proposed mappings, the Riemannian metric reduces to Euclidean inner product, which is much less computationally expensive. We focus on the Symmetric Positive Definite (SPD) manifolds which are beneficial in various fields such as data science and statistics. This work opens a research opportunity for extension of the proposed mappings to other well-known manifolds.

Index Terms—LBFGS, Riemannian optimization, positive definite manifolds, isometric vector transport, quasi-Newton’s method

I. INTRODUCTION

Various numerical optimization methods have appeared, for the Euclidean spaces, which can be categorized into first-order and second-order methods [1]. Examples for the former category are steepest descent and gradient descent and for the latter group are Newton’s method. Computation of the Hessian matrix is usually expensive in Newton’s method encouraging many practical problems to either use quasi-Newton’s methods for approximating the Hessian matrix or use non-linear conjugate gradient [2]. The most well-known algorithm for quasi-Newton optimization is Broyden–Fletcher–Goldfarb–Shanno (BFGS) [3]. Limited-memory BFGS (LBFGS) is a simplified version of BFGS which utilizes less memory [4], [5]. It has recursive unfoldings which approximate the descent directions in optimization.

Unlike Euclidean spaces in which the optimization direction lie in a linear coordinate system, Riemannian spaces

have curvature in coordinates. Recently, extension of optimization methods from Euclidean spaces to Riemannian manifolds has been extensively noticed in the literature [6], [7]. For example, Euclidean BFGS has been extended to Riemannian manifolds, named Riemannian BFGS (RBFGS), [8], its convergence has been proven [9], [10], and its properties have been analyzed in the literature [11]. As vector transport is computationally expensive in RBFGS, cautious RBFGS was proposed [12] which ignores the curvature condition in the Wolfe conditions [13] and only checks the Armijo condition [14]. Since the curvature condition guarantees that the approximation of Hessian remains positive definite, it compensates by checking a cautious condition [15] before updating the approximation of Hessian. This cautious RBFGS has been used in the Manopt optimization toolbox [16]. Another approach is an extension of the Euclidean LBFGS to Riemannian manifolds, named Riemannian LBFGS (RLBFGS), using both Wolfe conditions [13] in linesearch can be found in [17], [18], [19]. Some other direct extensions of Euclidean BFGS to Riemannian spaces exist (e.g., see [20, Chapter 7]).

In this paper, we address the computationally expensive parts of RLBFGS algorithm, which are computation of vector transports, their adjoints, and Riemannian metrics. To achieve this, we propose two mappings, in the tangent space, which make RLBFGS free of vector transport. We name the obtained algorithm Vector Transport Free (VTF)-RLBFGS. One mapping uses inverse second root and the other uses Cholesky decomposition which is very efficient [21]. The proposed mappings make both vector transport and adjoint vector transport, which are used in RLBFGS, identity. This reduction of transports to identity makes optimization much less expensive computationally. Moreover, as the vector transports become identity, they are isometric which is a suitable property mostly used in the convergence proofs of RBFGS and RLBFGS algorithms [9], [10]. Furthermore, under the proposed mappings, the Riemannian metric reduces to Euclidean inner product which is much less computationally expensive. In this paper, we concentrate on the Symmetric Positive Definite (SPD) manifolds [17], [18], [22] which are very useful in data science and machine

*The first two authors contributed equally to this work.

learning, such as in mixture models [19], [23]. This paper opens a new research path for extension of the proposed mappings to other well-known manifolds such as Grassmann and Stiefel [24].

The remainder of this paper is organized as follows. Section II reviews the notations and technical background on Euclidean LBFGS, Wolfe conditions, Riemannian LBFGS, and SPD manifold. The proposed mappings using inverse second root and Cholesky decomposition are introduced in Sections III and IV, respectively. Simulation results are reported in Section VI. Finally, Section VII concludes the paper and proposes the possible future directions.

II. BACKGROUND AND NOTATIONS

A. Euclidean BFGS and LBFGS

Consider minimization of the cost function $f(\Sigma)$ where the point Σ belongs to some domain. In Newton's method, the descent direction \mathbf{p}_k at the iteration k is calculated as [1]:

$$\mathbf{B}_k \mathbf{p}_k = -\nabla f(\Sigma_k) \implies \mathbf{p}_k = -\mathbf{B}_k^{-1} \nabla f(\Sigma_k), \quad (1)$$

where \mathbf{B}_k is the Hessian or approximation of Hessian and $\nabla f(\Sigma_k)$ is the gradient of function at iteration k . The Euclidean BFGS method is a quasi-Newton's method which approximates the Hessian matrix as [3], [1]:

$$\mathbf{B}_{k+1} := \mathbf{B}_k + \frac{\mathbf{y}_k \mathbf{y}_k^\top}{\mathbf{y}_k^\top \mathbf{s}_k} - \frac{\mathbf{B}_k \mathbf{s}_k \mathbf{s}_k^\top \mathbf{B}_k^\top}{\mathbf{s}_k^\top \mathbf{B}_k \mathbf{s}_k}, \quad (2)$$

where $\mathbf{s}_k := \Sigma_{k+1} - \Sigma_k$ and $\mathbf{y}_k := \nabla f(\Sigma_{k+1}) - \nabla f(\Sigma_k)$. The descent direction is then calculated using Eq. (1).

The Euclidean LBFGS calculates the descent direction recursively where it uses the approximation of the inverse Hessian as follows [4], [5]:

$$\mathbf{H}_{k+1} := \mathbf{V}_k^\top \mathbf{H}_k \mathbf{V}_k + \rho_k \mathbf{s}_k \mathbf{s}_k^\top, \quad (3)$$

where \mathbf{H}_k denotes the approximation of the inverse of the Hessian at iteration k , $\rho_k := 1/(\mathbf{y}_k^\top \mathbf{s}_k)$, and $\mathbf{V}_k := \mathbf{I} - \rho_k \mathbf{y}_k \mathbf{s}_k^\top$ in which \mathbf{I} denotes the identity matrix. The LBFGS algorithm updates the approximation of the inverse of the Hessian matrix recursively and for that it always stores a memory window of pairs $\{\mathbf{y}_k, \mathbf{s}_k\}$ [5].

B. Linesearch and Wolfe Conditions

After finding the descent direction \mathbf{p}_k at each iteration k of optimization, one needs to know what step size α_k should be taken in that direction. Linesearch should be performed to find the largest step, for faster progress, satisfying Wolfe conditions [13]:

$$f(\Sigma_k + \alpha_k) \leq f(\Sigma_k) + c_1 \alpha_k \mathbf{p}_k^\top \nabla f(\Sigma_k), \quad (4)$$

$$-\mathbf{p}_k^\top \nabla f(\Sigma_k + \alpha_k \mathbf{p}_k) \leq -c_2 \mathbf{p}_k^\top \nabla f(\Sigma_k), \quad (5)$$

where $0 < c_1 < c_2 < 1$ and are recommended to be $c_1 = 10^{-1}$ and $c_2 = 0.9$ [1]. The former condition is the Armijo condition to check if cost decreases sufficiently [14] while the latter is the curvature condition making sure that the slope is reduced sufficiently in a way that the approximation of

Hessian remains positive definite. Note that there also exists a strong curvature condition, i.e., $|\mathbf{p}_k^\top \nabla f(\Sigma_k + \alpha_k \mathbf{p}_k)| \leq c_2 |\mathbf{p}_k^\top \nabla f(\Sigma_k)|$.

C. Riemannian Notations

Consider a Riemannian manifold denoted by \mathcal{M} . At every point $\Sigma \in \mathcal{M}$, there is a tangent space to the manifold, denoted by $T_\Sigma \mathcal{M}$. A tangent space includes tangent vectors. We denote a tangent vector by ξ . For $\xi, \eta \in T_\Sigma \mathcal{M}$, a metric on this manifold is the inner product defined on manifold and is denoted by $g_\Sigma(\xi, \eta)$. Note that the gradient of a cost function, whose domain is a manifold, is a tangent vector in the tangent space and is denoted by $\nabla f(\Sigma)$ for point $\Sigma \in \mathcal{M}$. Vector transport is an operator which maps a tangent vector $\xi \in T_{\Sigma_1} \mathcal{M}$ from its tangent space at point Σ_1 to another tangent space at another point Σ_2 . We denote this vector transport by $\mathcal{T}_{\Sigma_1, \Sigma_2}(\xi) : T_{\Sigma_1} \mathcal{M} \mapsto T_{\Sigma_2} \mathcal{M}$. Now, consider a point Σ on a manifold \mathcal{M} and a descent direction ξ in the tangent space $T_\Sigma \mathcal{M}$. The retraction $\text{Ret}_\Sigma(\xi) : T_\Sigma \mathcal{M} \mapsto \mathcal{M}$ retracts or maps the direction ξ in the tangent space onto the manifold \mathcal{M} . The operator exponential map, denoted by $\text{Exp}_\Sigma(\xi)$, is also capable of this mapping by moving along the geodesic. One can use the second-order Taylor expansion of exponential map, which is positive-preserving [25] for the case of SPD manifold, for approximating the exponential map. In this paper, $\text{tr}(\cdot)$ denotes the trace of matrix.

D. Riemannian BFGS and LBFGS

The Riemannian extension of Euclidean BFGS (RBFBS) [8], [9], [10] performs updates of Hessian approximation by Eq. (2) using Riemannian operators. RBFBS methods check both Wolfe conditions, Eqs. (4) and (5), which are computationally expensive. Cautious RBFBS [12] ignores the curvature condition and only checks the Armijo condition for linesearch. However, for ensuring that the Hessian approximation remains positive definite, it checks a cautious condition [15] before updating the Hessian approximation.

Riemannian LBFGS [17], [18], [19] performs the recursions of LBFGS in the Riemannian space for finding the descent direction $\xi_k \in T_{\Sigma_k} \mathcal{M}$ and checks both Wolfe conditions in linesearch. In every iteration k of optimization, recursion starts with the direction $\mathbf{p} = -\nabla f(\Sigma_k)$. Let the recursive function $\text{GetDirection}(\mathbf{p}, k)$ returns the descent direction. Inside every step of this recursion, we have [19, Algorithm 3]:

$$\tilde{\mathbf{p}} := \mathbf{p} - \frac{g_{\Sigma_k}(\mathbf{s}_k, \mathbf{p})}{g_{\Sigma_k}(\mathbf{y}_k, \mathbf{s}_k)} \mathbf{y}_k, \quad (6)$$

$$\hat{\mathbf{p}} := \mathcal{T}_{\Sigma_{k-1}, \Sigma_k}(\text{GetDirection}(\mathcal{T}_{\Sigma_{k-1}, \Sigma_k}^*(\tilde{\mathbf{p}}), k-1)), \quad (7)$$

$$\text{return } \xi_k := \hat{\mathbf{p}} - \frac{g_{\Sigma_k}(\mathbf{y}_k, \hat{\mathbf{p}})}{g_{\Sigma_k}(\mathbf{y}_k, \mathbf{s}_k)} \mathbf{s}_k + \frac{g_{\Sigma_k}(\mathbf{s}_k, \mathbf{s}_k)}{g_{\Sigma_k}(\mathbf{y}_k, \mathbf{s}_k)} \mathbf{p}, \quad (8)$$

where, inspired by the introduced \mathbf{s}_k and \mathbf{y}_k for Euclidean

spaces, we have:

$$\Sigma_{k+1} := \text{Exp}_{\Sigma_k}(\alpha_k \xi_k) \text{ or } \text{Ret}_{\Sigma_k}(\alpha_k \xi_k), \quad (9)$$

$$s_{k+1} := \mathcal{T}_{\Sigma_k, \Sigma_{k+1}}(\alpha_k \xi_k), \quad (10)$$

$$y_{k+1} := \nabla f(\Sigma_{k+1}) - \mathcal{T}_{\Sigma_k, \Sigma_{k+1}}(\nabla f(\Sigma_k)). \quad (11)$$

Note that the new point in every iteration is found by retraction, or an exponential map, of the searched point along the descent direction onto manifold. According to Eq. (7) in recursion and Eq. (10), RLFBGS involves both adjoint vector transport and vector transport which are computationally expensive. Moreover, Eqs. (6) and (8) show that Riemannian metric is utilized many times inside recursions. Our proposed mappings in this paper simply all vector transport, adjoint vector transport, and metric which are used in the RLFBGS algorithm.

E. Symmetric Positive Definite (SPD) Manifold

Consider the SPD manifold [17], [18] whose every point is a SPD matrix, i.e., $\Sigma \in \mathcal{M}$ and $\mathbb{S}_{++}^n \ni \Sigma \succ \mathbf{0}$. It can be shown that the tangent space to the SPD manifold is the space of symmetric matrices, i.e., $T_{\mathcal{M}}(\Sigma) \subset \mathbb{S}_{++}^n$ [22]. In this paper, we focus on SPD manifolds which are widely used in data science. The operators for metric, gradient, exponential map, and vector transport on SPD manifolds are listed in Table I [18], [19]. In this table, $\nabla_E f(\Sigma)$ denotes the Euclidean gradient and L_1 and L_2 are the lower-triangular matrices in Cholesky decomposition of points Σ_1 and Σ_2 , respectively.

III. VECTOR TRANSPORT FREE RIEMANNIAN LFBGS USING MAPPING BY INVERSE SECOND ROOT

We propose two mappings on tangent vectors in the tangent space where the first mapping is by inverse second root. Our first proposed mapping in the tangent space of every point $\Sigma \in \mathcal{M}$ is:

$$\xi' := \Sigma^{-\frac{1}{2}} \xi \Sigma^{-\frac{1}{2}} \implies \xi = \Sigma^{\frac{1}{2}} \xi' \Sigma^{\frac{1}{2}}, \quad (12)$$

where the mapped tangent vector still remains in the tangent space, i.e. $\xi, \xi' \in T_{\Sigma} \mathcal{M} \subset \mathbb{S}_{++}^n$. It is important the proposed mapping is bijective and keeps the tangent vector in the tangent space while it simplifies vector transport, adjoint vector transport, and metric.

Under the proposed mapping (12), the Riemannian operators on a SPD manifold are modified and mostly simplified. These operators are listed in Table I. In the following, we provide proofs for these modifications.

Proposition 1: After mapping (12), the metric on SPD manifold is reduced to the Euclidean inner product, i.e.,

$$g_{\Sigma}(\xi', \eta') = \text{tr}(\xi' \eta'). \quad (13)$$

Proof:

$$\begin{aligned} g_{\Sigma}(\xi', \eta') &\stackrel{(a)}{=} \text{tr}(\Sigma^{-1} \xi \Sigma^{-1} \eta) = \text{tr}(\Sigma^{-\frac{1}{2}} \Sigma^{-\frac{1}{2}} \xi \Sigma^{-\frac{1}{2}} \Sigma^{-\frac{1}{2}} \eta) \\ &\stackrel{(b)}{=} \text{tr}(\underbrace{\Sigma^{-\frac{1}{2}} \xi \Sigma^{-\frac{1}{2}}}_{=\xi'} \underbrace{\Sigma^{-\frac{1}{2}} \eta \Sigma^{-\frac{1}{2}}}_{=\eta'}) \stackrel{(12)}{=} \text{tr}(\xi' \eta'), \end{aligned}$$

where (a) is because of definition of metric on SPD manifolds (see Table I) and (b) is thanks to the cyclic property of trace. Q.E.D. ■

Proposition 2: After mapping (12), the gradient on a SPD manifold is changed to:

$$\nabla' f(\Sigma) = \frac{1}{2} \Sigma^{\frac{1}{2}} (\nabla_E f(\Sigma) + (\nabla_E f(\Sigma))^{\top}) \Sigma^{\frac{1}{2}}, \quad (14)$$

where $\nabla_E f(\Sigma)$ denotes the Euclidean gradient.

Proof:

$$\begin{aligned} \nabla' f(\Sigma) &\stackrel{(12)}{=} \Sigma^{-\frac{1}{2}} \nabla f(\Sigma) \Sigma^{-\frac{1}{2}} \\ &\stackrel{(a)}{=} \frac{1}{2} \Sigma^{-\frac{1}{2}} \Sigma (\nabla_E f(\Sigma) + (\nabla_E f(\Sigma))^{\top}) \Sigma \Sigma^{-\frac{1}{2}} \\ &= \frac{1}{2} \Sigma^{\frac{1}{2}} (\nabla_E f(\Sigma) + (\nabla_E f(\Sigma))^{\top}) \Sigma^{\frac{1}{2}}, \end{aligned}$$

where (a) is due to definition of gradient on a SPD manifold (see Table I). Q.E.D. ■

Proposition 3: After mapping (12), the vector transport is changed to identity, i.e.,

$$\mathcal{T}'_{\Sigma_1, \Sigma_2}(\xi') = \xi', \quad (15)$$

hence, optimization becomes vector transport free.

Proof:

$$\begin{aligned} \mathcal{T}'_{\Sigma_1, \Sigma_2}(\xi') &\stackrel{(12)}{=} \Sigma_2^{-\frac{1}{2}} \mathcal{T}_{\Sigma_1, \Sigma_2}(\xi) \Sigma_2^{-\frac{1}{2}} \\ &\stackrel{(a)}{=} \underbrace{\Sigma_2^{-\frac{1}{2}} (\Sigma_2^{\frac{1}{2}} \Sigma_1^{-\frac{1}{2}} \xi \Sigma_1^{-\frac{1}{2}} \Sigma_2^{\frac{1}{2}})}_{=I} \Sigma_2^{-\frac{1}{2}} \\ &= \Sigma_1^{-\frac{1}{2}} \xi \Sigma_1^{-\frac{1}{2}} \stackrel{(12)}{=} \xi', \end{aligned}$$

where (a) is due to definition of vector transport on a SPD manifold (see Table I). Q.E.D. ■

Proposition 4: After mapping (12), the exponential map on a SPD manifold becomes:

$$\text{Exp}_{\Sigma}(\xi') = \Sigma^{\frac{1}{2}} \exp(\xi') \Sigma^{\frac{1}{2}}. \quad (16)$$

Proof:

$$\begin{aligned} \text{Exp}_{\Sigma}(\xi') &\stackrel{(a)}{=} \Sigma \exp(\Sigma^{-1} \xi) \stackrel{(b)}{=} \Sigma^{\frac{1}{2}} \exp(\Sigma^{-\frac{1}{2}} \xi \Sigma^{-\frac{1}{2}}) \Sigma^{\frac{1}{2}} \\ &\stackrel{(12)}{=} \Sigma^{\frac{1}{2}} \exp(\xi') \Sigma^{\frac{1}{2}}, \end{aligned}$$

where (a) is shown in [17, Eq. 3.3] and (b) is shown in [17, Eq. 3.2]. Also see Table I. Q.E.D. ■

Proposition 5: After mapping (12), the adjoint of vector transport on a SPD manifold remains the same. In other words, if before mapping we have the definition of adjoint vector transport as [9]:

$$g_{\Sigma_1}(\xi, \mathcal{T}_{\Sigma_1, \Sigma_2}^* \eta) = g_{\Sigma_2}(\mathcal{T}_{\Sigma_1, \Sigma_2} \xi, \eta), \quad (17)$$

$\forall \xi \in T_{\Sigma_1} \mathcal{M}, \forall \eta \in T_{\Sigma_2} \mathcal{M}$, we will have:

$$g_{\Sigma_1}(\xi', \mathcal{T}_{\Sigma_1, \Sigma_2}^{*'} \eta') = g_{\Sigma_2}(\mathcal{T}'_{\Sigma_1, \Sigma_2} \xi', \eta'), \quad (18)$$

$\forall \xi' \in T_{\Sigma_1} \mathcal{M}, \forall \eta' \in T_{\Sigma_2} \mathcal{M}$.

Corollary 1: It can be concluded directly from the definition, as well as Propositions 1, 3, and 5 that the adjoint of vector transport is again identity under mapping (12).

TABLE I
OPERATORS ON SPD MANIFOLD UNDER THE PROPOSED MAPPINGS.

Operator	No mapping
Metric, $g_{\Sigma}(\xi, \eta)$	$\text{tr}(\Sigma^{-1} \xi \Sigma^{-1} \eta)$
Gradient, $\nabla f(\Sigma)$	$\frac{1}{2} \Sigma (\nabla_E f(\Sigma) + (\nabla_E f(\Sigma))^{\top}) \Sigma$
Exponential map, $\text{Exp}_{\Sigma}(\xi)$	$\Sigma \exp(\Sigma^{-1} \xi) = \Sigma^{\frac{1}{2}} \exp(\Sigma^{-\frac{1}{2}} \xi \Sigma^{-\frac{1}{2}}) \Sigma^{\frac{1}{2}}$
Vector transport, $\mathcal{T}_{\Sigma_1, \Sigma_2}(\xi)$	$\Sigma_2^{\frac{1}{2}} \Sigma_1^{-\frac{1}{2}} \xi \Sigma_1^{-\frac{1}{2}} \Sigma_2^{\frac{1}{2}}$ or $L_2 L_1^{-1} \xi L_1^{-\top} L_2^{\top}$
Approx. Euclidean retraction, $\text{Ret}_{\Sigma}(\xi)$	$\Sigma + \xi + \frac{1}{2} \xi \Sigma^{-1} \xi$
Operator	Mapping by inverse second root
Mapping	$\xi' := \Sigma^{-\frac{1}{2}} \xi \Sigma^{-\frac{1}{2}}$
Metric, $g'_{\Sigma}(\xi', \eta')$	$\text{tr}(\xi' \eta')$
Gradient, $\nabla' f(\Sigma)$	$\frac{1}{2} \Sigma^{\frac{1}{2}} (\nabla_E f(\Sigma) + (\nabla_E f(\Sigma))^{\top}) \Sigma^{\frac{1}{2}}$
Exponential map, $\text{Exp}_{\Sigma}(\xi')$	$\Sigma^{\frac{1}{2}} \exp(\xi') \Sigma^{\frac{1}{2}}$
Vector transport, $\mathcal{T}'_{\Sigma_1, \Sigma_2}(\xi')$	ξ'
Approx. Euclidean retraction, $\text{Ret}_{\Sigma}(\xi')$	$\Sigma + \Sigma^{\frac{1}{2}} \xi' \Sigma^{\frac{1}{2}} + \frac{1}{2} \Sigma^{\frac{1}{2}} \xi'^2 \Sigma^{\frac{1}{2}}$
Operator	Mapping by Cholesky decomposition
Mapping	$\xi' := L^{-1} \xi L^{-\top}$
Metric, $g'_{\Sigma}(\xi', \eta')$	$\text{tr}(\xi' \eta')$
Gradient, $\nabla' f(\Sigma)$	$\frac{1}{2} L^{\top} (\nabla_E f(\Sigma) + (\nabla_E f(\Sigma))^{\top}) L$
Exponential map, $\text{Exp}_{\Sigma}(\xi')$	$\Sigma \exp(L^{-\top} \xi' L^{\top})$
Vector transport, $\mathcal{T}'_{\Sigma_1, \Sigma_2}(\xi')$	ξ'
Approx. Euclidean retraction, $\text{Ret}_{\Sigma}(\xi')$	$\Sigma + L \xi' L^{\top} + \frac{1}{2} L \xi'^2 L^{\top}$

Proposition 6: After mapping (12), the approximation of Euclidean retraction, using second-order Taylor expansion, on a SPD manifold becomes:

$$\text{Ret}_{\Sigma}(\xi') = \Sigma + \Sigma^{\frac{1}{2}} \xi' \Sigma^{\frac{1}{2}} + \frac{1}{2} \Sigma^{\frac{1}{2}} \xi'^2 \Sigma^{\frac{1}{2}}. \quad (19)$$

Proof:

$$\begin{aligned} \text{Ret}_{\Sigma}(\xi') &\stackrel{(a)}{=} \Sigma + \xi + \frac{1}{2} \xi \Sigma^{-1} \xi \\ &\stackrel{(12)}{=} \Sigma + \Sigma^{\frac{1}{2}} \xi' \Sigma^{\frac{1}{2}} + \frac{1}{2} \Sigma^{\frac{1}{2}} \xi' \underbrace{\Sigma^{-1} \Sigma^{\frac{1}{2}} \Sigma^{\frac{1}{2}}}_{=I} \xi' \Sigma^{\frac{1}{2}} \\ &= \Sigma + \Sigma^{\frac{1}{2}} \xi' \Sigma^{\frac{1}{2}} + \frac{1}{2} \Sigma^{\frac{1}{2}} \xi'^2 \Sigma^{\frac{1}{2}}, \end{aligned}$$

where (a) is because of approximation of Euclidean retraction, using the second-order Taylor expansion, on SPD manifolds (see Table I). Q.E.D. ■

IV. VECTOR TRANSPORT FREE RIEMANNIAN LBFSGS USING MAPPING BY CHOLESKY DECOMPOSITION

Our second proposed mapping is by Cholesky decomposition which is very efficient computationally. Consider the Cholesky decomposition of point $\Sigma \in \mathcal{M}$ [21]:

$$\mathbf{0} \prec \Sigma = LL^{\top} \implies \Sigma^{-1} = L^{-\top} L^{-1}, \quad (20)$$

where $L \in \mathbb{R}^{n \times n}$ is the lower-triangular matrix in Cholesky decomposition. It is noteworthy that many of the MATLAB matrix multiplication operators, which the Manopt toolbox

[16] also uses, apply Cholesky decomposition internally due to its efficiency.

In the tangent space of every point $\Sigma \in \mathcal{M}$, the proposed mapping is:

$$\xi' := L^{-1} \xi L^{-\top} \implies \xi = L \xi' L^{\top}, \quad (21)$$

where $\xi, \xi' \in T_{\Sigma} \mathcal{M} \subset \mathbb{S}_{++}^n$. Note that, similar to the previous mapping, the tangent matrix is still symmetric under this mapping; hence, it remains in the tangent space of the SPD manifold [22]. Similar to the previous mapping, under the second proposed mapping (12), the Riemannian operators on SPD manifold are simplified. These operators can be found in Table I. In the following, we provide proofs for these operators.

Proposition 7: After mapping (21), the metric on a SPD manifold is reduced to the Euclidean inner product, i.e.,

$$g_{\Sigma}(\xi', \eta') = \text{tr}(\xi' \eta'). \quad (22)$$

Proof:

$$\begin{aligned} g_{\Sigma}(\xi', \eta') &\stackrel{(a)}{=} \text{tr}(\Sigma^{-1} \xi \Sigma^{-1} \eta) = \text{tr}(L^{-\top} L^{-1} \xi L^{-\top} L^{-1} \eta) \\ &\stackrel{(b)}{=} \text{tr}(\underbrace{L^{-1} \xi L^{-\top}}_{=\xi'} \underbrace{L^{-1} \eta L^{-\top}}_{=\eta'}) \stackrel{(21)}{=} \text{tr}(\xi' \eta'), \end{aligned}$$

where (a) is because of definition of metric on SPD manifolds (see Table I) and (b) is thanks to the cyclic property of trace. Q.E.D. ■

Proposition 8: After mapping (21), the gradient on SPD manifold is changed to:

$$\nabla' f(\Sigma) = \frac{1}{2} \mathbf{L}^\top (\nabla_E f(\Sigma) + (\nabla_E f(\Sigma))^\top) \mathbf{L}, \quad (23)$$

where $\nabla_E f(\Sigma)$ denotes the Euclidean gradient.

Proof:

$$\begin{aligned} \nabla' f(\Sigma) &\stackrel{(21)}{=} \mathbf{L}^{-1} \nabla f(\Sigma) \mathbf{L}^{-\top} \\ &\stackrel{(a)}{=} \frac{1}{2} \mathbf{L}^{-1} \Sigma (\nabla_E f(\Sigma) + (\nabla_E f(\Sigma))^\top) \Sigma \mathbf{L}^{-\top} \\ &\stackrel{(20)}{=} \frac{1}{2} \mathbf{L}^{-1} \mathbf{L} \mathbf{L}^\top (\nabla_E f(\Sigma) + (\nabla_E f(\Sigma))^\top) \mathbf{L} \mathbf{L}^\top \mathbf{L}^{-\top} \\ &= \frac{1}{2} \mathbf{L}^\top (\nabla_E f(\Sigma) + (\nabla_E f(\Sigma))^\top) \mathbf{L}, \end{aligned}$$

where (a) is due to definition of gradient on a SPD manifold (see Table I). Q.E.D. ■

Proposition 9: After mapping (21), the vector transport is changed to identity, i.e.,

$$\mathcal{T}'_{\Sigma_1, \Sigma_2}(\xi') = \xi', \quad (24)$$

hence, optimization becomes vector transport free.

Proof:

$$\begin{aligned} \mathcal{T}'_{\Sigma_1, \Sigma_2}(\xi') &\stackrel{(21)}{=} \mathbf{L}_2^{-1} \mathcal{T}_{\Sigma_1, \Sigma_2}(\xi) \mathbf{L}_2^{-\top} \\ &\stackrel{(a)}{=} \underbrace{\mathbf{L}_2^{-1} (\mathbf{L}_2 \mathbf{L}_1^{-1} \xi \mathbf{L}_1^{-\top} \mathbf{L}_2^\top)}_{=I} \underbrace{\mathbf{L}_2^{-\top}}_{=I} \\ &= \mathbf{L}_1^{-1} \xi \mathbf{L}_1^{-\top} \stackrel{(21)}{=} \xi', \end{aligned}$$

where (a) is due to definition of vector transport on SPD manifold (see Table I). Q.E.D. ■

Proposition 10: After mapping (21), the exponential map on SPD manifold becomes:

$$\text{Exp}_\Sigma(\xi') = \Sigma \exp(\mathbf{L}^{-\top} \xi' \mathbf{L}^\top). \quad (25)$$

Proof:

$$\begin{aligned} \text{Exp}_\Sigma(\xi') &\stackrel{(a)}{=} \Sigma \exp(\Sigma^{-1} \xi) \stackrel{(b)}{=} \Sigma \exp(\mathbf{L}^{-\top} \underbrace{\mathbf{L}^{-1} \mathbf{L}}_{=I} \xi' \mathbf{L}^\top) \\ &= \Sigma \exp(\mathbf{L}^{-\top} \xi' \mathbf{L}^\top), \end{aligned}$$

where (a) is shown in [17, Eq. 3.3] and (b) is because of Eqs. (20) and (21). Q.E.D. ■

Similar to Proposition 5 and Corollary 1, the adjoint vector transport becomes identity under mapping (21).

Proposition 11: After mapping (21), the approximation of Euclidean retraction by second-order Taylor expansion on a SPD manifold becomes:

$$\text{Ret}_\Sigma(\xi') = \Sigma + \mathbf{L} \xi' \mathbf{L}^\top + \frac{1}{2} \mathbf{L} \xi'^2 \mathbf{L}^\top. \quad (26)$$

Proof:

$$\begin{aligned} \text{Ret}_\Sigma(\xi') &\stackrel{(a)}{=} \Sigma + \xi + \frac{1}{2} \xi \Sigma^{-1} \xi \stackrel{(b)}{=} \Sigma + \mathbf{L} \xi' \mathbf{L}^\top \\ &\quad + \frac{1}{2} \mathbf{L} \xi' \underbrace{\mathbf{L}^\top \mathbf{L}^{-\top}}_{=I} \underbrace{\mathbf{L}^{-1} \mathbf{L}}_{=I} \xi' \mathbf{L}^\top, \end{aligned}$$

```

1 Input: Initial point  $\Sigma_0$ 
2  $\mathbf{H}_0 \leftarrow \frac{1}{\sqrt{g'_{\Sigma_0}(\nabla' f(\Sigma_0), \nabla' f(\Sigma_0))}} \mathbf{I}$ 
3 for  $k = 0, 1, \dots$  do
4   Compute  $\nabla' f(\Sigma_k)$  from Euclidean gradient by
   one of the mappings in Table I
5    $\xi'_k \leftarrow \text{GetDirection}(-\nabla' f(\Sigma_k), k)$ 
6    $\alpha_k \leftarrow \text{Line search with Wolfe conditions}$ 
7    $\Sigma_{k+1} \leftarrow \text{Exp}_{\Sigma_k}(\alpha_k \xi'_k)$  or  $\text{Ret}_{\Sigma_k}(\alpha_k \xi'_k)$ 
8    $s'_{k+1} \leftarrow \mathcal{T}'_{\Sigma_k, \Sigma_{k+1}}(\alpha_k \xi'_k)$ 
9    $y'_{k+1} \leftarrow \nabla' f(\Sigma_{k+1}) - \mathcal{T}'_{\Sigma_k, \Sigma_{k+1}}(\nabla' f(\Sigma_k))$ 
10   $\mathbf{H}_{k+1} \leftarrow \frac{g'_{\Sigma_{k+1}}(s'_{k+1}, y'_{k+1})}{g'_{\Sigma_{k+1}}(y'_{k+1}, y'_{k+1})}$ 
11  Store  $y'_{k+1}$ ,  $s'_{k+1}$ ,  $g'_{\Sigma_{k+1}}(s'_{k+1}, y'_{k+1})$ ,
    $g'_{\Sigma_{k+1}}(s'_{k+1}, s'_{k+1})$ , and  $\mathbf{H}_{k+1}$ 
12 return  $\Sigma_{k+1}$ 
13
14 Function  $\text{GetDirection}(p', k)$ 
15 if  $k > 0$  then
16    $\tilde{p}' \leftarrow p' - \frac{g'_{\Sigma_k}(s'_k, p')}{g'_{\Sigma_k}(y'_k, s'_k)} y'_k$ 
17    $\tilde{p}' \leftarrow \mathcal{T}'_{\Sigma_{k-1}, \Sigma_k}(\text{GetDirection}(\mathcal{T}'_{\Sigma_{k-1}, \Sigma_k}(\tilde{p}'), k-1))$ 
18   return  $\tilde{p}' - \frac{g'_{\Sigma_k}(y'_k, \tilde{p}')}{g'_{\Sigma_k}(y'_k, s'_k)} s'_k + \frac{g'_{\Sigma_k}(s'_k, s'_k)}{g'_{\Sigma_k}(y'_k, s'_k)} p'$ 
19 else
20   return  $\mathbf{H}_0 p'$ 

```

Algorithm 1: The VTF-RLBFGS algorithm

which gives Eq. (26), where (a) is because of approximation of Euclidean retraction, using second-order Taylor expansion, on SPD manifolds (see Table I), and (b) is because of Eqs. (20) and (21). Q.E.D. ■

Noticing Eq. (21), the approximation of retraction under mapping by Cholesky decomposition, i.e. Eq. (26), can be restated as $\text{Ret}_\Sigma(\xi') = 0.5 \Sigma + 0.5 \mathbf{L}(\mathbf{I} + \xi')^2 \mathbf{L}^\top$. Defining $\Psi := \mathbf{L}(\mathbf{I} + \xi')$ restates this retraction as $\text{Ret}_\Sigma(\xi') = 0.5 \Sigma + 0.5 \Psi \Psi^\top$ because ξ' is symmetric. The term $\Psi \Psi^\top$ is very efficient and fast to compute because it is symmetric.

Corollary 2: Following Proposition 3, Corollary 1, and Proposition 9, we see that under mapping (12) or (21), both vector transport and adjoint vector transport are identity. As these transforms become identity, they also become isometric because inner products of vectors do not change under these transforms. As they are identity, these transforms also preserve the length of vectors under the proposed mappings.

Propositions 1 and 7 and Corollary 2 show the two proposed mappings simplify vector transport and adjoint vector transport to isometric identity and reduce the Riemannian metric to Euclidean inner product. These reductions and simplifications reduce computations significantly during optimization on the manifold. The VTF-RLBFGS algorithm using either of the proposed mappings is shown in Algorithm 1.

V. ANALYTICAL DISCUSSION AND COMPLEXITY ANALYSIS

Lemma 1: Vector transport is valid under both proposed mappings (12) and (20) because they preserve the properties of vector transport.

Proof: A valid vector transport should satisfy three properties [19] (also see [6, Definition 8.1.1] [7, Definition 10.62]):

- 1) The following property:

$$\exists v \in T_{\Sigma_1} \mathcal{M} : \mathcal{T}_{\Sigma_1, \Sigma_2}(\xi) \in T_{\text{Ret}_{\Sigma}(v)} \mathcal{M}, \forall \xi \in T_{\Sigma_1} \mathcal{M},$$

holds because the tangent space $T_{\text{Ret}_{\Sigma}(v)} \mathcal{M}$ is isomorphic to the space of symmetric matrices and the identity vector transports return the tangent vector itself which is in the space of symmetric matrices.

- 2) The vector transport of a tangent vector from one point to itself should be the same tangent vector. This holds because vector transport is identity under the proposed mappings:

$$\mathcal{T}_{\Sigma, \Sigma}(\xi) = \xi, \forall \xi \in T_{\Sigma_1} \mathcal{M}$$

- 3) The vector transport $\mathcal{T}_{\Sigma_1, \Sigma_2}(\xi)$ should be linear which is because it is equal to ξ under the proposed mappings.

As after applying the mappings, the vector transport holds the three above properties, it is a valid transport. Q.E.D. ■

Proposition 12: The time complexity of the recursion part in RLFBFGS is improved from $\mathcal{O}(kn^3)$ and $\Omega(kn^3)$ to $\mathcal{O}(kn^2)$ and $\Omega(kn^2)$ after applying mapping (12) or (20).

Proof:

– **Upper bound analysis:** The most time consuming part of the RLFBFGS algorithm is the recursive function `GetDirection(.)` defined in Section 2.4. In every call of recursion, Eqs. (6)-(8) are performed. The metric used in Eqs. (6) and (8) takes $\mathcal{O}(n^3)$ and $\mathcal{O}(n^2)$ before and after applying the mappings, respectively (cf. Table I). This is because matrix inversion takes $\mathcal{O}(n^3)$ time and the matrices are vectorized within trace operator in the algorithm implementation. The vector transport used in Eq. (7) takes $\mathcal{O}(n^3)$ and $\mathcal{O}(1)$ before and after applying the mappings, respectively (cf. Table I). Recursion in RLFBFGS is usually done for a constant k number of times [9]. Overall, the complexity of recursion is $\mathcal{O}(kn^3)$ and $\mathcal{O}(kn^2)$, for RLFBFGS with and without mappings, respectively. Hence, our proposed mappings improve the time of optimization. This time improvement shows off better if computation of gradients in Eq. (11) is not dominant in complexity.

– **Lower bound analysis:** Computing matrix inversion in the metric before applying our mappings (cf. Table I) takes $\Omega(n^2 \log n)$ [26] while metric takes $\Omega(n^2)$ after the mappings. The vector transport takes $\Omega(n^3)$ and $\Omega(1)$ before and after the mappings, respectively. Overall, the complexity of recursion is $\Omega(kn^3)$ and $\Omega(kn^2)$, for RLFBFGS with and without mappings, respectively. Hence, our mappings improve the time of optimization in the best case as well as the worst case. ■

VI. SIMULATIONS

In this section, we evaluate the effectiveness of the proposed mappings, i.e. (12) and (21), in the tangent space. Here, we show that these mappings often improve the performance and speed of RLFBFGS. The code of this article is available in <https://github.com/bghojogh/LBFGS-Vector-Transport-Free>.

A. Optimization Problem

The optimization problem, which we selected for evaluation, is the Riemannian optimization for Gaussian Mixture Model (GMM) without the use of expectation maximization. We employ RLFBFGS with and without the proposed mappings for fitting the GMM problem whose algorithm can be found in [19], [23]. This is a suitable problem for evaluation of the proposed mappings because the covariance matrices are SPD [22]. For this, we minimize the negative log-likelihood of GMM where the covariance matrix is constrained to belong to the SPD matrix manifold [19]. For n -dimensional GMM, the optimization problem is:

$$\begin{aligned} & \underset{\{\alpha_j, \mu_j, \Sigma_j\}_{j=1}^K}{\text{minimize}} && - \sum_{i=1}^N \log \left(\sum_{j=1}^K \alpha_j \mathcal{N}(\mathbf{x}_i; \mu_j, \Sigma_j) \right), \\ & \text{subject to} && \Sigma_j \in \mathcal{M} = \mathbb{S}_{++}^n, \quad \forall j \in \{1, \dots, K\}, \end{aligned} \quad (27)$$

where N denotes the sample size, K denotes the number of components in mixture model, and α_j , μ_j , and Σ_j are the mixing probability, mean, and covariance of the j -th component, respectively. We use the same reformulation trick of [19] to reformulate the cost function of (27).

B. Experimental Setup

We solved the optimization problem (27) using RLFBFGS which is focused in this paper. For all experiments, with and without the proposed mappings, we use both Wolfe line-search conditions. The mixture parameters were initialized using K-means++ [27] following [19]. Three different levels of separation of Gaussian models, namely low, mid, and high, were used. The reader can refer to [19] for mathematical details of these separation levels. For every experiment, we performed optimization for ten runs and the reported results are the average of performances over the runs. In our reports, we denote the proposed Vector Transport Free (VTF) RLFBFGS with VTF-RLFBFGS where ISR and Cholesky (or Chol.) stand for VTF-RLFBFGS using mapping by inverse second root and Cholesky decomposition, respectively. The programming language, used for experiments, was MATLAB and the hardware was Intel Core-i7 CPU with the base frequency 2.20 GHz and 12 GB RAM.

C. Evaluation of the Proposed Mappings

The average number of iterations, convergence time, time per iteration, and the cost value of last iteration are reported in Tables II and III where exponential map is used in former and Taylor approximation of exponential map is used for retraction in the latter. In these experiments, we report performances for $K \in \{2, 5\}$, $n \in \{2, 10\}$, $N = 10n^2 \in$

TABLE II

COMPARISON OF AVERAGE RESULTS OVER TEN RUNS WHERE EXPONENTIAL MAP IS USED IN ALGORITHMS AND $K \in \{2, 5\}$, $n \in \{2, 10\}$,
 $N = 10n^2 \in \{40, 1000\}$.

K	n	Separation	Algorithm	#iters	conv. time	iter. time	last cost
2	2	Low	VTF (ISR)	53.100±18.248	68.380±52.834	1.140±0.504	0.364±0.444
			VTF (Chol.)	52.100±17.866	61.096±48.433	1.030±0.463	0.364±0.444
			RLBFGS	52.500±16.595	65.890±49.208	1.125±0.458	0.364±0.444
		Mid	VTF (ISR)	56.400±21.813	76.124±69.189	1.150±0.574	0.657±0.344
			VTF (Chol.)	54.400±19.156	68.456±64.290	1.099±0.504	0.638±0.333
			RLBFGS	57.700±19.844	81.957±64.463	1.250±0.550	0.657±0.344
		High	VTF (ISR)	25.500±3.064	9.518±2.922	0.366±0.067	0.341±0.371
			VTF (Chol.)	26.000±4.738	10.254±5.468	0.377±0.108	0.341±0.371
			RLBFGS	25.500±3.064	10.054±3.141	0.386±0.073	0.341±0.371
	10	Low	VTF (ISR)	77.600±54.175	235.615±466.119	1.936±1.751	4.210±0.889
			VTF (Chol.)	84.100±73.260	313.398±714.908	2.041±2.150	4.209±0.889
			RLBFGS	77.600±52.754	242.743±458.641	2.069±1.733	4.209±0.889
		Mid	VTF (ISR)	44.600±7.260	43.654±16.872	0.948±0.208	4.262±1.098
			VTF (Chol.)	45.900±8.647	45.661±20.088	0.955±0.236	4.262±1.098
			RLBFGS	45.200±8.080	48.104±19.981	1.025±0.243	4.262±1.098
		High	VTF (ISR)	44.400±9.252	43.684±22.460	0.936±0.254	3.874±1.395
			VTF (Chol.)	47.100±8.333	48.278±21.112	0.987±0.240	3.874±1.395
			RLBFGS	43.300±7.150	43.904±17.626	0.981±0.225	3.874±1.395
5	2	Low	VTF (ISR)	152.400±62.819	1344.573±999.949	7.560±3.406	0.260±0.458
			VTF (Chol.)	174.800±114.139	2168.886±3090.820	8.680±6.348	0.265±0.466
			RLBFGS	166.300±76.884	1767.676±1406.454	8.788±4.427	0.267±0.454
		Mid	VTF (ISR)	120.700±69.620	942.713±1063.075	5.807±3.877	0.781±0.207
			VTF (Chol.)	121.600±65.030	897.110±988.826	5.720±3.445	0.781±0.207
			RLBFGS	136.300±91.493	1404.654±1986.798	7.057±5.378	0.764±0.225
		High	VTF (ISR)	46.400±17.322	94.741±105.045	1.739±0.902	1.805±0.385
			VTF (Chol.)	46.200±19.803	98.065±122.950	1.729±1.020	1.805±0.385
			RLBFGS	46.200±18.937	104.934±126.734	1.879±1.064	1.805±0.385
	10	Low	VTF (ISR)	295.900±86.577	5524.495±3173.855	17.299±5.221	6.175±0.745
			VTF (Chol.)	292.300±83.828	5294.565±3165.735	16.737±5.350	6.197±0.718
			RLBFGS	318.800±100.216	7083.082±4801.718	20.279±6.859	6.173±0.744
		Mid	VTF (ISR)	134.200±54.956	1139.332±919.917	7.302±3.227	6.753±0.708
			VTF (Chol.)	133.300±52.415	1100.519±842.840	7.183±3.045	6.753±0.708
			RLBFGS	135.300±54.965	1268.707±967.678	8.070±3.580	6.753±0.708
		High	VTF (ISR)	68.600±12.367	241.487±87.593	3.398±0.764	6.599±0.836
			VTF (Chol.)	74.000±14.071	279.271±105.828	3.632±0.838	6.599±0.836
			RLBFGS	68.300±11.982	258.475±93.959	3.661±0.790	6.599±0.836

$\{40, 1000\}$. For the sake of fairness, all the three compared algorithms start with the same initial points in every run. The reader can see more extensive experiments for more sample size and dimensionality, i.e. $K \in \{2, 5\}$, $n \in \{2, 10, 100\}$, $N = 100n^2 \in \{400, 10000, 1000000\}$, in the Supplementary Material.

1) *Discussion by Varying Separability:* As Tables II and III show, the proposed ISR mapping converges faster than no mapping most often in all separability levels. Both its time per iteration and number of iterations are often less than no mapping. These tables also show that the proposed Cholesky mapping converges faster than no mapping in most of the cases, although not all cases. Overall, we see that the two proposed mappings make RLBFGS faster and more efficient most often. This pacing improvement can be noticed more

for low and mid separability levels because they are harder cases to converge.

In terms of quality of local minimum, the proposed mappings often find the same local minimum as no mapping, but in a faster way. The equality of the found local optima in the three methods is because of using the same RLBFGS algorithm as their base in addition to having the same initial points. In some cases, the proposed mappings have even found better local minima.

2) *Discussion by Varying Dimensionality:* We can discuss the results of Tables II and III by varying dimensionality, $n \in \{2, 10\}$. Tables IV and V in Supplementary Material also report performance for dimensions $n \in \{2, 10, 100\}$ for larger sample size. Obviously, by increasing dimensionality, the time of convergence goes up and the faster pacing of the

TABLE III

COMPARISON OF AVERAGE RESULTS OVER TEN RUNS WHERE RETRACTION WITH TAYLOR SERIES EXPANSION IS USED IN ALGORITHMS AND $K \in \{2, 5\}$, $n \in \{2, 10\}$, $N = 10n^2 \in \{40, 1000\}$.

K	n	Separation	Algorithm	#iters	conv. time	iter. time	last cost
2	2	Low	VTF (ISR)	59.800±22.553	93.135±88.437	1.320±0.711	0.610±0.366
			VTF (Chol.)	62.600±29.079	106.545±117.633	1.355±0.830	0.619±0.382
			RLBFGS	59.800±26.803	100.424±120.310	1.363±0.787	0.610±0.366
		Mid	VTF (ISR)	45.800±16.982	48.155±38.045	0.900±0.454	0.482±0.497
			VTF (Chol.)	47.000±18.074	51.529±41.465	0.930±0.483	0.482±0.497
			RLBFGS	45.000±16.330	48.150±37.285	0.921±0.458	0.482±0.497
		High	VTF (ISR)	25.600±4.142	9.816±3.837	0.370±0.093	0.270±0.456
			VTF (Chol.)	26.300±4.448	10.540±4.190	0.385±0.101	0.270±0.456
			RLBFGS	25.500±4.353	10.526±4.819	0.396±0.113	0.270±0.456
	10	Low	VTF (ISR)	75.800±25.607	166.736±137.600	1.955±0.816	4.129±0.771
			VTF (Chol.)	74.500±22.629	152.074±107.531	1.855±0.682	4.129±0.771
			RLBFGS	74.800±25.442	172.641±143.198	2.054±0.834	4.129±0.771
		Mid	VTF (ISR)	50.900±13.956	64.501±38.055	1.170±0.395	3.472±1.154
			VTF (Chol.)	52.100±13.892	66.775±41.257	1.184±0.410	3.472±1.154
			RLBFGS	51.000±14.063	70.132±46.421	1.264±0.450	3.472±1.154
		High	VTF (ISR)	43.600±5.522	42.763±11.897	0.963±0.168	4.353±1.081
			VTF (Chol.)	47.400±6.620	50.438±15.187	1.041±0.182	4.353±1.081
			RLBFGS	44.300±6.464	47.830±14.747	1.055±0.192	4.353±1.081
5	2	Low	VTF (ISR)	262.500±126.532	4430.577±4455.877	13.849±6.991	0.082±0.281
			VTF (Chol.)	253.500±124.970	4086.076±3967.586	13.084±6.850	0.099±0.279
			RLBFGS	270.700±144.145	5305.821±5495.383	15.560±8.452	0.090±0.282
		Mid	VTF (ISR)	110.900±50.886	731.318±769.639	5.445±2.806	1.010±0.349
			VTF (Chol.)	112.200±60.736	792.756±1053.832	5.436±3.358	1.010±0.349
			RLBFGS	111.900±55.183	814.994±975.737	5.827±3.289	1.010±0.349
		High	VTF (ISR)	52.000±13.565	116.485±69.535	2.071±0.728	1.626±0.431
			VTF (Chol.)	51.400±12.616	114.032±67.916	2.057±0.735	1.626±0.431
			RLBFGS	53.400±14.081	139.989±89.213	2.408±0.936	1.626±0.431
	10	Low	VTF (ISR)	219.700±57.908	2946.040±1513.372	12.579±3.507	6.643±0.662
			VTF (Chol.)	226.100±86.010	3272.111±2808.634	12.707±5.156	6.625±0.650
			RLBFGS	231.300±64.484	3607.215±1947.580	14.516±4.305	6.642±0.663
		Mid	VTF (ISR)	87.100±21.502	413.616±223.510	4.458±1.310	6.585±0.569
			VTF (Chol.)	87.200±21.186	405.484±214.985	4.374±1.262	6.585±0.569
			RLBFGS	87.400±20.403	454.434±227.556	4.918±1.339	6.585±0.569
		High	VTF (ISR)	60.500±10.533	181.113±76.070	2.892±0.649	6.827±0.836
			VTF (Chol.)	62.700±11.295	197.565±93.653	3.019±0.827	6.827±0.836
			RLBFGS	58.900±11.040	187.518±86.254	3.058±0.746	6.827±0.836

proposed mappings is noticed more compared to no mapping.

3) Discussion by Varying the Number of Components:

The results of Tables II and III can also be interpreted based on varying the number of mixture components, $K \in \{2, 5\}$. The more number of components makes the optimization problem harder. Hence, the difference of speeds of the proposed mappings and no mapping can be noticed more for $K = 5$; although, for both K values, the proposed mappings are often faster than no mapping.

4) Discussion by Varying Retraction Type:

We can also compare the performance of algorithms in terms of type of retraction. Tables II and III report performances where exponential map and Taylor approximation of exponential map are used for retraction, respectively. Comparing these tables shows that using Taylor approximation usually con-

verges faster than using exponential map which makes sense because exponential map requires passing on geodesics. This difference of pacing is more obvious for larger number of components, i.e., $K = 5$. Our two proposed mappings outperform no mapping for both types retraction. This shows that our mappings are effective regardless of the details of operators.

5) Discussion by Varying the Sample Size:

Tables II and III report for $n \in \{2, 10\}$, $N = 10n^2 \in \{40, 1000\}$. More experiments for larger sample size and dimensionality, i.e. $K \in \{2, 5\}$, $n \in \{2, 10, 100\}$, $N = 100n^2 \in \{400, 10000, 1000000\}$, can be found in Tables IV and V in the Supplementary Material. Comparing those tables with Tables II and III shows that larger sample size and/or dimensionality takes more time to converge as expected.

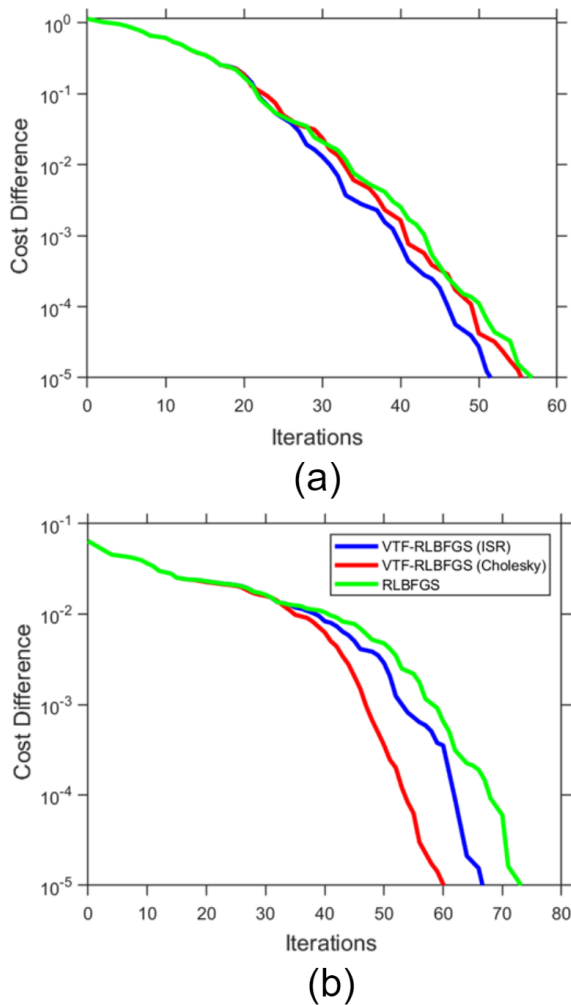


Fig. 1. The cost difference progress for several runs: (a) $K = 2$, $n = 10$, $N = 1000$, mid separation, with exponential map, and (b) $K = 2$, $n = 2$, $N = 400$, mid separation, with exponential map.

Still, our proposed mappings often converge faster than no mapping. The difference of pacing is mostly less in larger sample size compared to smaller sample size. This is because very large sample size consumes time on computation of cost function and the difference is not given much chance to show off in that case.

6) *Discussion by Cost Difference Progress:* The log-scale cost difference progress of several insightful runs of RLBFGS, with and without the proposed mappings, are illustrated in Fig. 1. A complete set of plots for cost difference progress can be seen in Figs. 2, 3, 4, and 5 in the Supplementary Material. Figs. 1-a and 1-b show that in some cases, ISR mapping is faster than the Cholesky mapping and in some other cases, we have the other way around.

VII. CONCLUSION AND FUTURE DIRECTION

In this paper, we proposed two mappings in the tangent space of SPD manifolds by inverse second root and Cholesky decomposition. The proposed mappings simplify the vector transports and adjoint vector transports to identity. These

transports are widely used in RLBFGS quasi-Newton optimization, to identity. They also reduce the Riemannian metric to the Euclidean inner product which is more efficient computationally. Simulation results verified the effectiveness of the proposed mappings for an optimization task on SPD matrix manifolds. In this work, we focused on mappings for SPD manifolds which are widely used in machine learning and data science. A possible future direction is to extend the proposed mappings for other well-known Riemannian manifolds, such as Grassmann and Stiefel [24], as well as other Riemannian optimization methods. This paper opens a new research path for such mappings in the tangent space and we conjecture that such mappings can make numerical Riemannian optimization more efficient.

REFERENCES

- [1] J. Nocedal and S. Wright, *Numerical optimization*. Springer Science & Business Media, 2006.
- [2] M. R. Hestenes and E. Stiefel, *Methods of conjugate gradients for solving linear systems*. NBS Washington, DC, 1952, vol. 49, no. 1.
- [3] R. Fletcher, *Practical methods of optimization*. John Wiley & Sons, 2013.
- [4] J. Nocedal, "Updating quasi-Newton matrices with limited storage," *Mathematics of computation*, vol. 35, no. 151, pp. 773–782, 1980.
- [5] D. C. Liu and J. Nocedal, "On the limited memory BFGS method for large scale optimization," *Mathematical programming*, vol. 45, no. 1, pp. 503–528, 1989.
- [6] P.-A. Absil, R. Mahony, and R. Sepulchre, *Optimization algorithms on matrix manifolds*. Princeton University Press, 2009.
- [7] N. Boumal, *An introduction to optimization on smooth manifolds*. Available online, 2020.
- [8] C. Qi, K. A. Gallivan, and P.-A. Absil, "Riemannian BFGS algorithm with applications," in *Recent advances in optimization and its applications in engineering*. Springer, 2010, pp. 183–192.
- [9] W. Ring and B. Wirth, "Optimization methods on Riemannian manifolds and their application to shape space," *SIAM Journal on Optimization*, vol. 22, no. 2, pp. 596–627, 2012.
- [10] W. Huang, K. A. Gallivan, and P.-A. Absil, "A Broyden class of quasi-Newton methods for Riemannian optimization," *SIAM Journal on Optimization*, vol. 25, no. 3, pp. 1660–1685, 2015.
- [11] M. Seibert, M. Kleinsteuber, and K. Hüper, "Properties of the BFGS method on Riemannian manifolds," *Mathematical System Theory C Festschrift in Honor of Uwe Helmke on the Occasion of his Sixtieth Birthday*, pp. 395–412, 2013.
- [12] W. Huang, P.-A. Absil, and K. A. Gallivan, "A Riemannian BFGS method for nonconvex optimization problems," in *Numerical Mathematics and Advanced Applications ENUMATH 2015*. Springer, 2016, pp. 627–634.
- [13] P. Wolfe, "Convergence conditions for ascent methods," *SIAM Review*, vol. 11, no. 2, pp. 226–235, 1969.
- [14] L. Armijo, "Minimization of functions having Lipschitz continuous first partial derivatives," *Pacific Journal of mathematics*, vol. 16, no. 1, pp. 1–3, 1966.
- [15] D.-H. Li and M. Fukushima, "On the global convergence of the BFGS method for nonconvex unconstrained optimization problems," *SIAM Journal on Optimization*, vol. 11, no. 4, pp. 1054–1064, 2001.
- [16] N. Boumal, B. Mishra, P.-A. Absil, and R. Sepulchre, "Manopt, a Matlab toolbox for optimization on manifolds," *The Journal of Machine Learning Research*, vol. 15, no. 1, pp. 1455–1459, 2014.
- [17] S. Sra and R. Hosseini, "Conic geometric optimization on the manifold of positive definite matrices," *SIAM Journal on Optimization*, vol. 25, no. 1, pp. 713–739, 2015.
- [18] —, "Geometric optimization in machine learning," in *Algorithmic Advances in Riemannian Geometry and Applications*. Springer, 2016, pp. 73–91.
- [19] R. Hosseini and S. Sra, "An alternative to EM for Gaussian mixture models: batch and stochastic Riemannian optimization," *Mathematical Programming*, vol. 181, no. 1, pp. 187–223, 2020.
- [20] H. Ji, "Optimization approaches on smooth manifolds," Ph.D. dissertation, Australian National University, 2007.

- [21] G. H. Golub and C. F. Van Loan, *Matrix computations*. JHU press, 2013, vol. 3.
- [22] R. Bhatia, *Positive definite matrices*. Princeton University Press, 2009.
- [23] R. Hosseini and M. Mash'al, "Mixest: An estimation toolbox for mixture models," *arXiv preprint arXiv:1507.06065*, 2015.
- [24] A. Edelman, T. A. Arias, and S. T. Smith, "The geometry of algorithms with orthogonality constraints," *SIAM journal on Matrix Analysis and Applications*, vol. 20, no. 2, pp. 303–353, 1998.
- [25] B. Jeuris, R. Vandebril, and B. Vandereycken, "A survey and comparison of contemporary algorithms for computing the matrix geometric mean," *Electronic Transactions on Numerical Analysis*, vol. 39, no. ARTICLE, pp. 379–402, 2012.
- [26] A. Tveit, "On the complexity of matrix inversion," Norwegian University of Science and Technology, Trondheim, Tech. Rep., 2003.
- [27] D. Arthur and S. Vassilvitskii, "k-means++: The advantages of careful seeding," in *Proceedings of the eighteenth annual ACM-SIAM symposium on Discrete algorithms*, 2007, pp. 1027–1035.

Supplementary Materials

SIMULATIONS FOR LARGER SAMPLE SIZE AND DIMENSIONALITY

Tables IV and V report the average simulation results for large sample size, i.e., $N = 100n^2$. In these tables, exponential map and Taylor approximation for retraction are used, respectively. We also have reported results for large dimensionality $d = 100$ in these two tables.

COST DIFFERENCE PROGRESS FOR $N = 10n^2$ SAMPLE SIZE SIMULATIONS

The log-scale cost difference for simulations of $N = 10n^2$ are depicted in Figs. 2 and 3 for $K = 2$ and $K = 5$, respectively.

COST DIFFERENCE PROGRESS FOR $N = 100n^2$ SAMPLE SIZE SIMULATIONS

The log-scale cost difference for simulations of $N = 10n^2$ are depicted in Figs. 4 and 5 where exponential map and Taylor approximation for retraction are used, respectively.

TABLE IV

COMPARISON OF AVERAGE RESULTS OVER TEN RUNS WHERE EXPONENTIAL MAP IS USED IN ALGORITHMS AND $n \in \{2, 10, 100\}$,
 $N = 100n^2 \in \{400, 10000, 1000000\}$, $K = 2$.

n	Separation	Algorithm	#iters	conv. time	iter. time	last cost
2	Low	VTF (ISR)	72.000±22.949	127.902±98.372	1.616±0.584	0.281±0.394
		VTF (Chol.)	69.800±23.136	116.250±86.811	1.490±0.590	0.281±0.394
		RLBFGS	68.900±24.875	123.064±105.594	1.561±0.694	0.281±0.394
	Mid	VTF (ISR)	59.400±16.460	78.124±53.880	1.210±0.421	0.520±0.392
		VTF (Chol.)	54.900±12.862	63.241±34.382	1.082±0.332	0.516±0.393
		RLBFGS	58.400±17.037	80.042±62.183	1.240±0.497	0.520±0.392
	High	VTF (ISR)	23.300±2.627	7.434±2.288	0.313±0.057	0.102±0.288
		VTF (Chol.)	22.900±2.685	7.273±2.084	0.312±0.052	0.102±0.288
		RLBFGS	23.300±2.497	7.917±2.135	0.335±0.053	0.102±0.288
10	Low	VTF (ISR)	63.400±16.728	112.682±74.903	1.664±0.489	4.364±1.299
		VTF (Chol.)	65.000±17.994	117.215±82.258	1.670±0.538	4.364±1.299
		RLBFGS	64.900±17.866	126.987±87.668	1.819±0.561	4.364±1.299
	Mid	VTF (ISR)	48.200±8.766	58.096±23.089	1.164±0.256	4.024±1.627
		VTF (Chol.)	49.800±11.811	64.021±34.770	1.208±0.364	4.024±1.627
		RLBFGS	48.400±10.906	64.099±32.746	1.251±0.361	4.024±1.627
	High	VTF (ISR)	45.100±7.385	49.628±20.550	1.065±0.243	3.290±1.129
		VTF (Chol.)	47.800±8.121	55.217±22.622	1.117±0.251	3.290±1.129
		RLBFGS	45.200±7.131	52.883±20.627	1.137±0.236	3.290±1.129
100	Low	VTF (ISR)	131.900±32.402	54826.327±30454.295	389.761±121.060	63.703±2.843
		VTF (Chol.)	141.200±36.908	59082.278±32385.087	392.658±110.916	63.703±2.843
		RLBFGS	136.300±36.059	56627.788±32602.224	387.367±119.404	63.703±2.843
	Mid	VTF (ISR)	87.800±20.225	23635.623±11743.237	259.026±52.061	61.263±4.734
		VTF (Chol.)	95.800±25.170	28033.655±16196.321	278.456±64.670	61.263±4.734
		RLBFGS	94.900±25.653	28527.524±17341.755	284.548±69.821	61.263±4.734
	High	VTF (ISR)	97.000±24.240	29048.836±12857.812	286.602±63.250	61.241±3.991
		VTF (Chol.)	105.100±27.477	33967.543±15707.841	308.668±70.065	61.241±3.991
		RLBFGS	103.200±26.389	33101.986±15790.066	305.002±74.361	61.241±3.991

TABLE V

COMPARISON OF AVERAGE RESULTS OVER TEN RUNS WHERE RETRACTION WITH TAYLOR SERIES EXPANSION IS USED IN ALGORITHMS AND $n \in \{2, 10, 100\}$, $N = 100n^2 \in \{400, 10000, 1000000\}$, $K = 2$.

n	Separation	Algorithm	#iters	conv. time	iter. time	last cost
2	Low	VTF (ISR)	79.800±49.973	206.935±343.153	1.839±1.340	0.403±0.578
		VTF (Chol.)	72.200±20.004	125.636±83.113	1.608±0.536	0.402±0.576
		RLBFGS	83.900±51.054	237.936±364.382	2.064±1.412	0.404±0.578
	Mid	VTF (ISR)	48.100±12.688	49.277±30.486	0.946±0.334	0.196±0.436
		VTF (Chol.)	50.100±14.271	56.329±40.420	1.017±0.422	0.196±0.436
		RLBFGS	51.000±13.622	61.036±39.550	1.099±0.412	0.196±0.436
	High	VTF (ISR)	25.300±3.945	9.887±3.903	0.377±0.101	0.111±0.261
		VTF (Chol.)	26.500±4.927	11.003±5.644	0.395±0.124	0.111±0.261
		RLBFGS	25.100±4.012	10.203±4.224	0.392±0.106	0.111±0.261
10	Low	VTF (ISR)	65.500±18.435	123.552±77.898	1.747±0.560	4.164±1.142
		VTF (Chol.)	66.500±19.558	122.281±79.423	1.688±0.569	4.164±1.142
		RLBFGS	65.200±18.743	130.098±84.241	1.835±0.622	4.164±1.142
	Mid	VTF (ISR)	40.600±5.211	38.915±12.591	0.938±0.177	4.589±1.278
		VTF (Chol.)	41.000±5.538	38.732±12.699	0.924±0.171	4.589±1.278
		RLBFGS	40.400±6.186	41.513±15.303	0.998±0.213	4.589±1.278
	High	VTF (ISR)	44.400±6.310	46.957±15.325	1.032±0.198	3.786±1.113
		VTF (Chol.)	46.000±6.616	50.393±15.950	1.070±0.195	3.786±1.113
		RLBFGS	44.200±7.099	50.707±18.070	1.116±0.222	3.786±1.113
100	Low	VTF (ISR)	118.500±11.404	39986.299±6719.992	335.341±26.657	62.241±5.708
		VTF (Chol.)	124.400±11.157	42882.658±7219.289	342.538±28.830	62.241±5.708
		RLBFGS	122.100±11.657	41702.121±7476.586	339.099±29.920	62.241±5.708
	Mid	VTF (ISR)	103.800±24.679	32533.037±16124.089	297.268±76.267	60.256±3.662
		VTF (Chol.)	111.900±28.781	37328.925±18924.066	314.512±82.724	60.256±3.662
		RLBFGS	112.100±28.769	39648.561±19857.076	333.549±90.495	60.256±3.662
	High	VTF (ISR)	96.300±25.880	28818.656±14923.845	283.824±67.267	60.601±4.436
		VTF (Chol.)	103.900±26.126	33669.987±16494.757	308.353±73.281	60.601±4.436
		RLBFGS	103.100±24.897	32849.937±16282.988	303.484±72.501	60.601±4.436

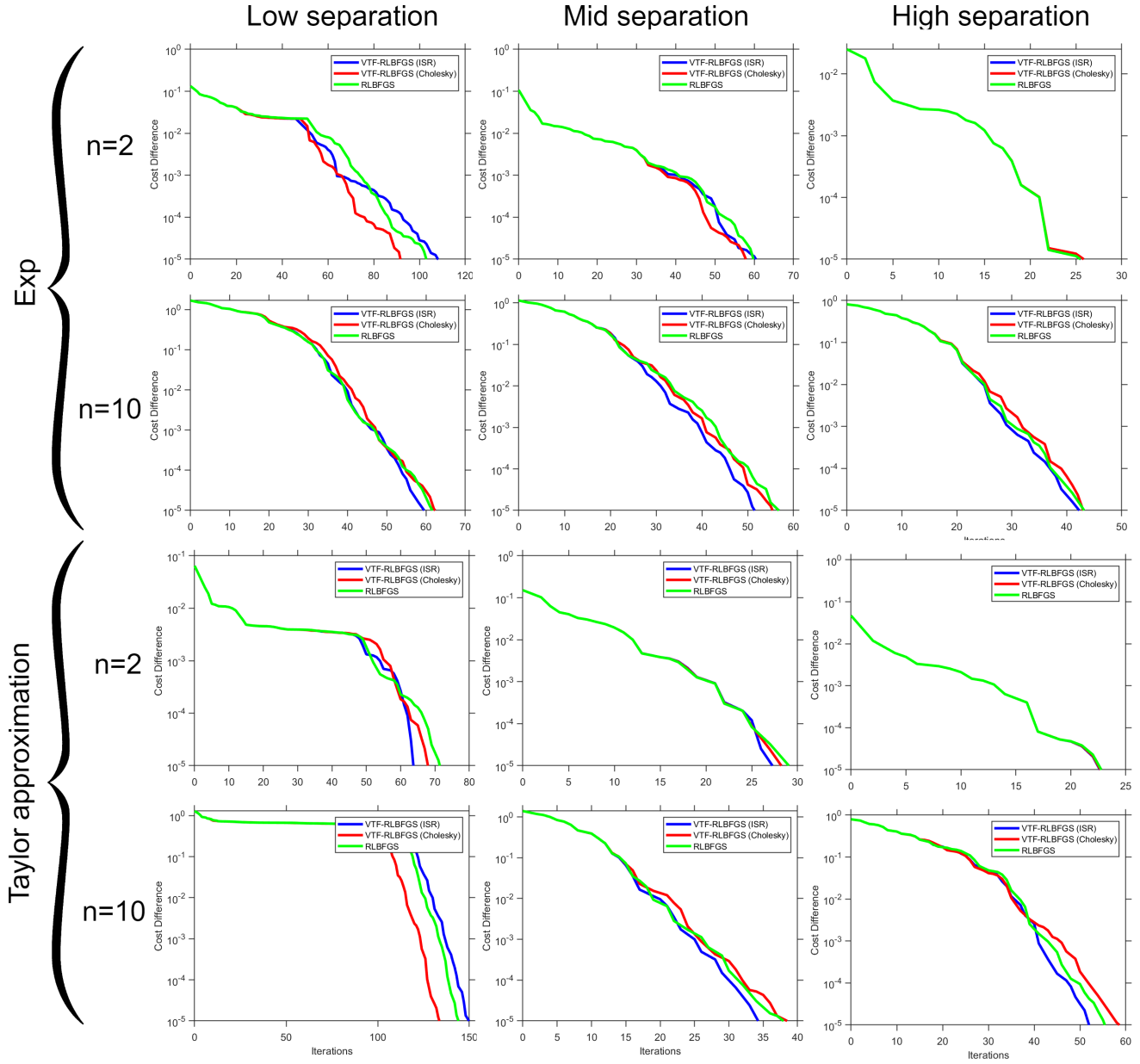


Fig. 2. Comparison of the proposed VTF-RLBFGS algorithm (using ISR and Cholesky) with RLBFGS in their cost differences. In these experiments, we had $K = 2$.

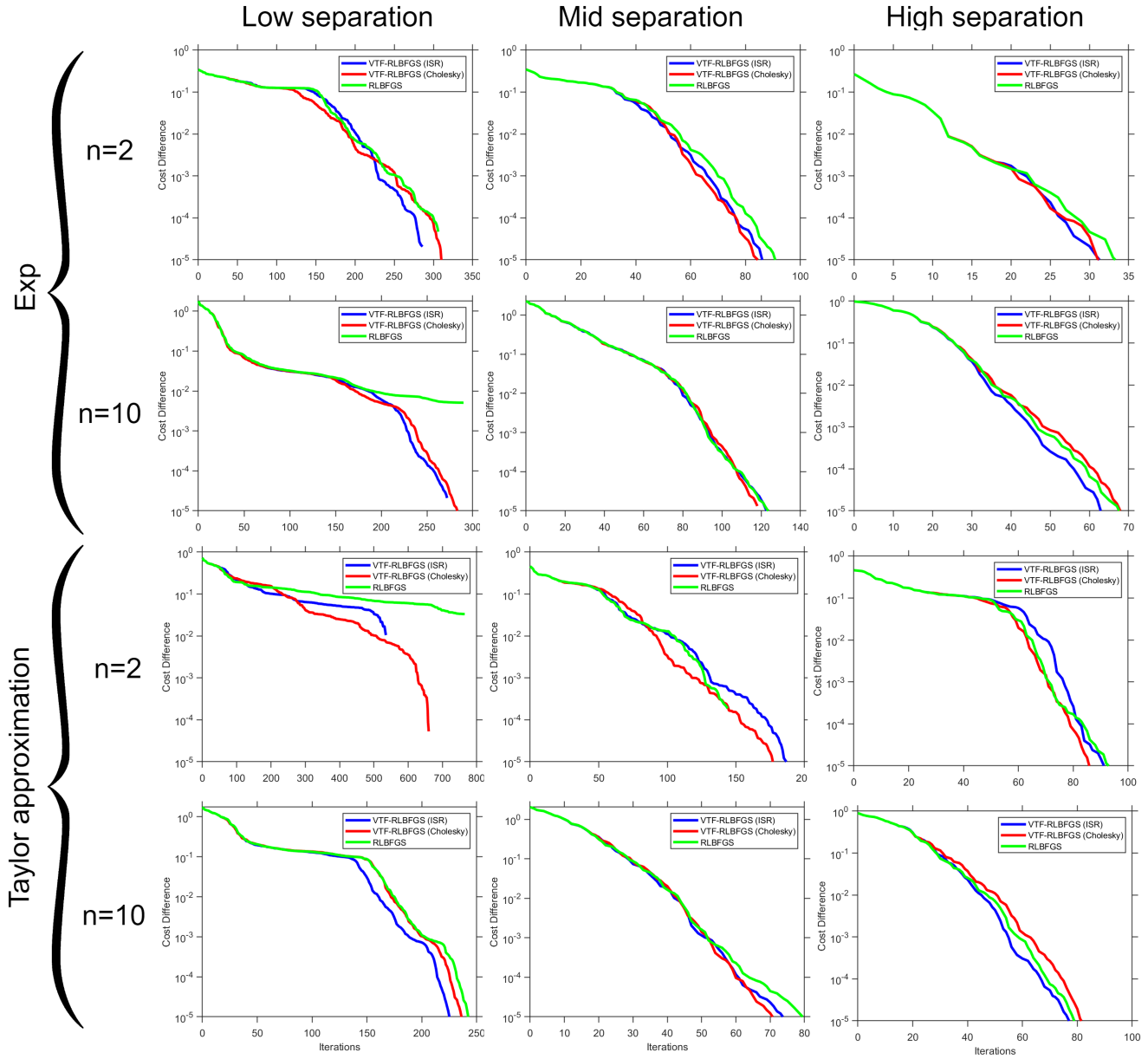


Fig. 3. Comparison of the proposed VTF-RLBFGS algorithm (using ISR and Cholesky) with RLBFGS in their cost differences. In these experiments, we had $K = 5$.

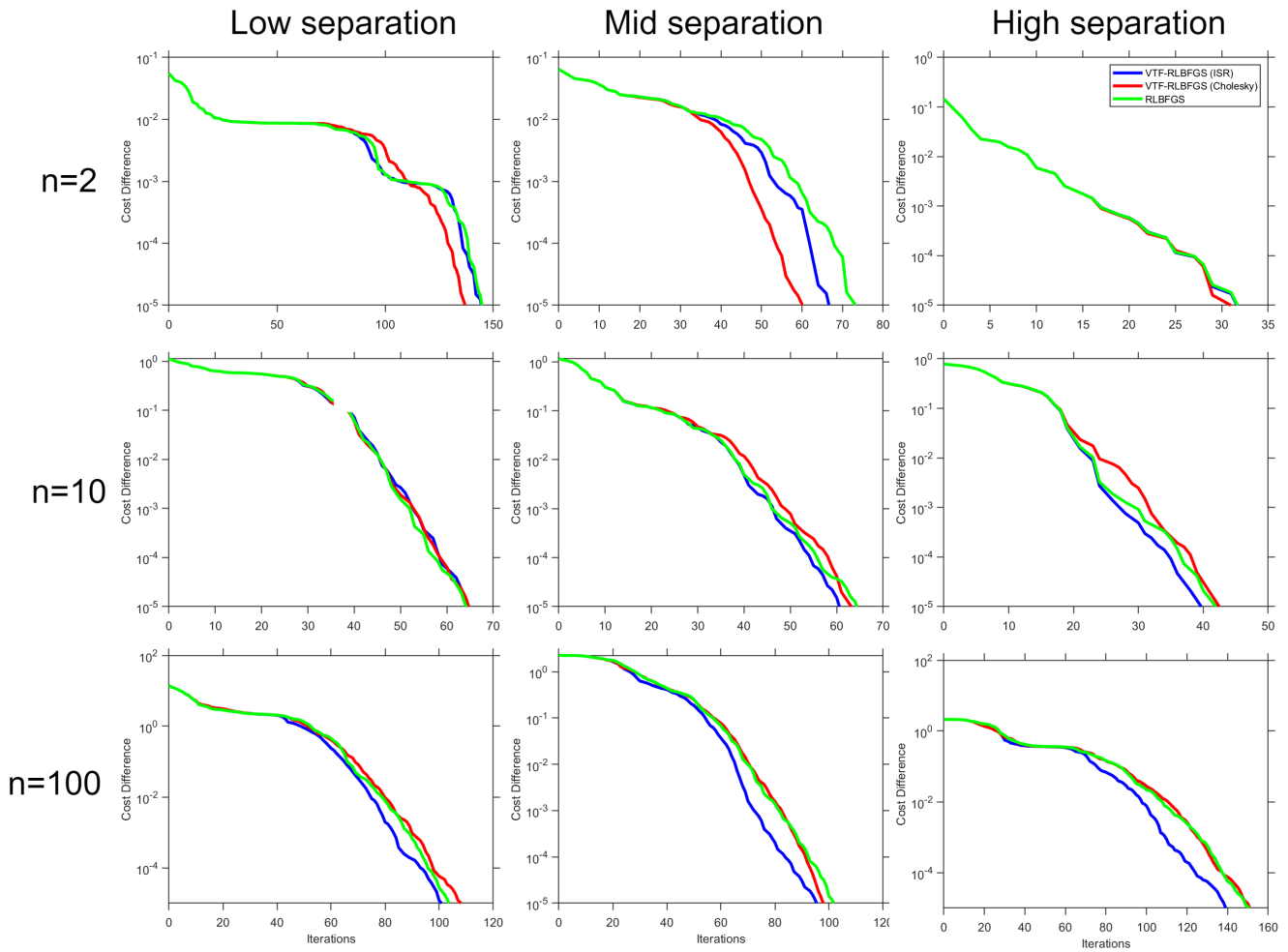


Fig. 4. Comparison of the proposed VTF-RLBFGS algorithm (using ISR and Cholesky) with RLBFGS in their cost differences. In these experiments, exponential map is used in optimization procedure and we had $K = 2$.

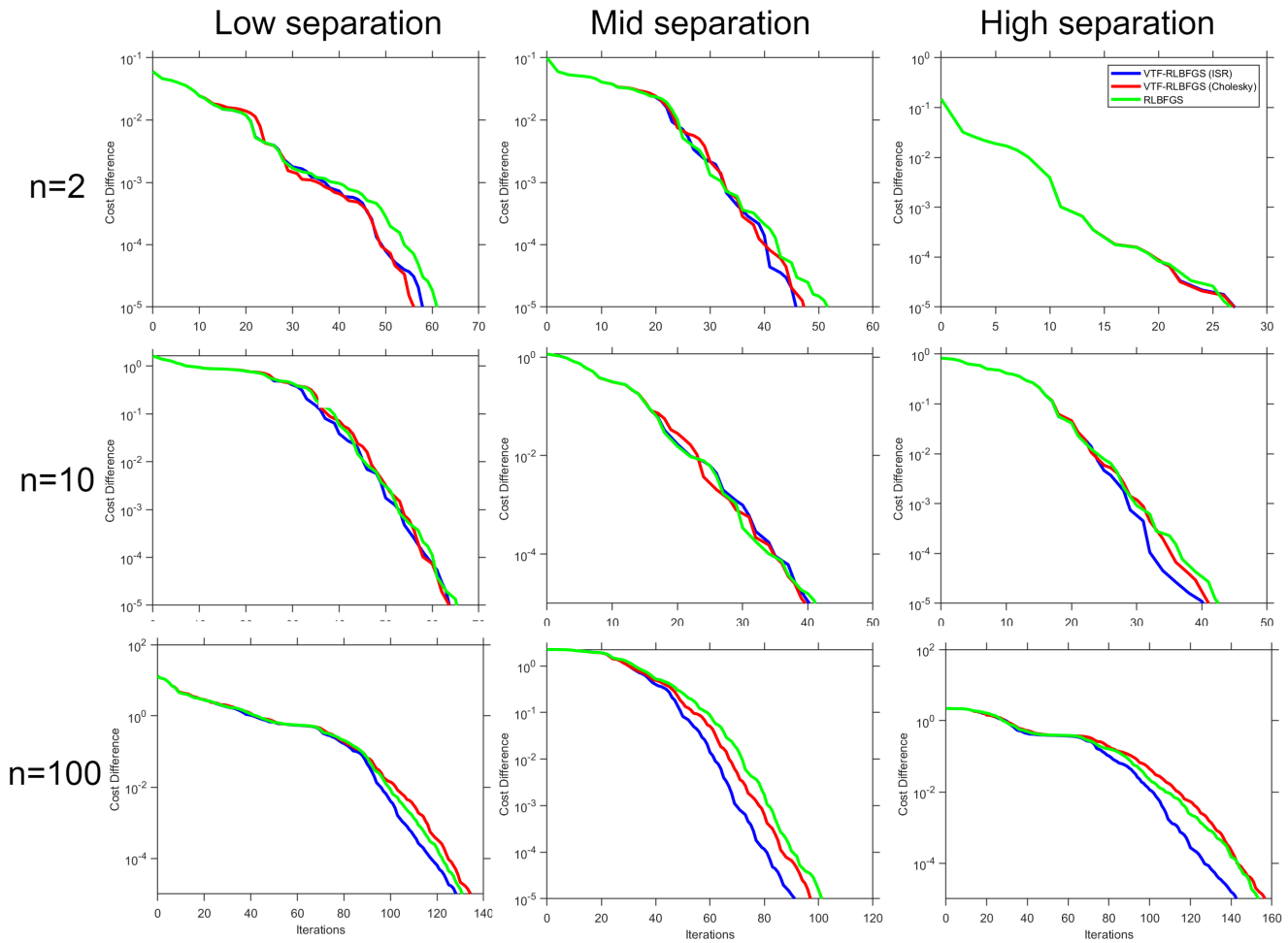


Fig. 5. Comparison of the proposed VTF-RLBFGS algorithm (using ISR and Cholesky) with RLBFGS in their cost differences. In these experiments, Taylor series expansion is used for approximation of retraction operator and we had $K = 2$.